ACS APPLIED MATERIALS & INTERFACES

Research Article

www.acsami.org

Hindered Disulfide Bonds to Regulate Release Rate of Model Drug from Mesoporous Silica

Peter Nadrah,[†] Uroš Maver,[†,§] Anita Jemec,[†,#] Tatjana Tišler,[†] Marjan Bele,[†,‡,⊥] Goran Dražić,[†,⊥,∥] Mojca Benčina,[†,¶] Albin Pintar,[†,‡,△] Odon Planinšek,[□] and Miran Gaberščček*[,†,‡,△]

[†]National Institute of Chemistry, Hajdrihova ul. 19, SI-1001 Ljubljana, Slovenia

[‡]Centre of Excellence for Low-Carbon Technologies, Hajdrihova ul. 19, SI-1001 Ljubljana, Slovenia

[⊥]Center of Excellence on Nanoscience and Nanotechnology − Nanocenter, Jamova c. 39, SI-1000 Ljubljana, Slovenia

[∥]Jožef Stefan Institute, Jamova c. 39, SI-1000 Ljubljana, Slovenia

[¶]EN-FIST Centre of Excellence, Dunajska c. 156, SI-1000 Ljubljana, Slovenia

[△]Faculty of Chemistry and Chemical Technology, University of Ljubljana, Aškerčeva c. 5, SI-1001 Ljubljana, Slovenia

[□]Faculty of Pharmacy, University of Ljubljana, Aškerčeva c. 7, SI-1000 Ljubljana, Slovenia

Supporting Information

ABSTRACT: With the advancement of drug delivery systems based on mesoporous silica nanoparticles (MSNs), a simple and efficient method regulating the drug release kinetics is needed. We developed redox-responsive release systems with three levels of hindrance around the disulfide bond. A model drug (rhodamine B dye) was loaded into MSNs' mesoporous voids. The pore opening was capped with β-cyclodextrin in order to prevent leakage of drug. Indeed, in absence of a reducing agent the systems exhibited little leakage, while the addition of dithiothreitol cleaved the disulfide bonds and enabled the release of cargo. The release rate and the amount of released dye were tuned by the level of hindrance around disulfide bonds, with the increased hindrance causing a decrease in the release rate as well as in the amount of released drug. Thus, we demonstrated the ability of the present mesoporous systems to intrinsically control the release rate and the amount of the released cargo by only minor structural variations. Furthermore, an *in vivo* experiment on zebrafish confirmed that the present model delivery system is nonteratogenic.

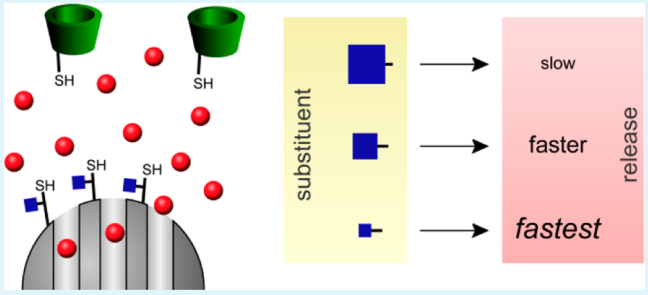

KEYWORDS: *drug delivery, mesoporous silica, nanoparticles, redox, controlled release*

INTRODUCTION

Stimulus-controlled drug delivery systems based on mesoporous silica is an emerging field with its beginnings in 2003.[1,2] MCM-41 type of mesoporous silica nanoparticles (MSNs) has been thoroughly studied and proved to be biocompatible.[3] The material offers a rigid and versatile basis for a delivery system with large surface area and ordered mesoporous structure.[4] Mesopores, according to IUPAC[5] defined as pores with a diameter of 2−50 nm, can be used to store drug molecules, whereas the ease of functionalization of silica surface provides a means to achieve controlled release of cargo molecules.[6] Construction of structures on the surface of MSNs in a gatelike fashion provides a precise control of the transport of the molecules between the inside of the pores and the surrounding medium.[6,7] Over the years, such gated systems evolved from those operating in organic solvents to systems able to function in cellular environments[8] and exhibiting great biocompatibility. Gatelike assemblies (capping agents) keep the drug molecules inside mesopores until the onset of a stimulus, such as pH change,[9,10] introduction of reducing agents,[11,12] light,[13,14] temperature change,[15] enzymes,[16] etc., at which point the drug molecules are released into the medium. The molecules, now free from their host, can interact with their pharmacological target. MSNs are a delivery system that protects the incorporated drug from enzymatic degradation, while simultaneously protecting the tissue from the drug's unwanted side effects.

An important aspect of drug delivery is also the rate with which the drug is released from its carrier. Different release rates enable tuning of the drug effect, achieving either a fast onset of the effect or a slow onset with a longer duration. The former is required in application of anesthetics, whereas a prolonged duration of drug effect and a constant drug plasma concentration are beneficial characteristics for antibiotic applications.

Received: February 16, 2013
Accepted: April 12, 2013
Published: April 12, 2013

There have been many attempts to control the release rate from a mesoporous support. The effect of pore diameter on the release kinetics has been well studied.[17−20] Another route to tune the kinetics is functionalization of silica surface with organic groups.[21] Controlling the release rate from mesoporous silica by alkyl chain functionalization was reported by Doadrio et al.[22] and Aznar et al.[23] The latter used different lengths of alkyl chains to slow down the diffusion process of the model drug incorporated into mesopores. Longer alkyl chains provided a slower release of cargo than their shorter counterparts. However, the release started as soon as MSNs came in contact with water, i.e., no stimulus-induced mechanism over release was used.

In stimulus-induced release systems based on MSNs the strength (concentration) or type of the stimulus influences the release rate of the cargo.[12,24−29] This kind of control of the release rate is externally driven (in respect to the mesoporous system). There is an obvious advantage of having a system that can dictate the release rate and the amount of drug released, while still being responsive to the external stimulus. Systems incorporating this kind of responsiveness have occasionally been reported. For example, Porta et al.[11] tuned the release rate of fluorescein by increasing the length of the linker connecting a peptide and α-cyclodextrin to the silica surface. In another study, Bernardos et al.[30] demonstrated the dependence of release profiles on the type of hydrolyzed starch derivative used to cap the pores and the cargo inside. Gruenhagen et al.[31] achieved variations in release profiles of ATP by using capping agents of different sizes. Xing et al.[32] achieved variations in the release rate of ibuprofen by varying the concentration of the pH-sensitive polymer Eudragit-S100 on mesoporous silica microparticles.

Drug delivery systems incorporating disulfide bonds hold promising features for intracellular delivery of drugs. Disulfide bond, while relatively stable in plasma,[33] is cleaved in intracellular fluid with tripeptide glutathione (GSH), because of the high GSH concentration in intracellular fluid (1−10 mM) compared to the lower concentration in plasma (0.002 mM).[34] Drug delivery systems responsive to GSH concentration change could retain the drug while being trafficked through the plasma and release the drug once it enters the cell. Delivery into cells is an especially important aspect for delivery of genetic material and drugs with intracellular targets. By varying the substituents close to the disulfide bond, Thorpe et al. showed it is possible to achieve different half-lives of disulfide bond cleavage.[35] Later, they also demonstrated improved antitumor effects of immunotoxins bearing a hindered disulfide bond compared to the unhindered one.[36] Recently, Kellogg et al. reported antibody−maytansinoid conjugates with varying hindrance surrounding the disulfide bond.[37] Indeed, a higher hindrance decreased the rate of disulfide reduction. Steric hindrance of disulfide bond connecting MSNs with a capping agent that keeps drug molecules inside the pores could provide a way to regulate the release rate of drug with intrinsic property of the system, while being responsive to endogenous stimulus at the same time. Thus, small variations in the structure of delivery system could provide different release profiles of the same drug in the same environmental conditions.

An important property of novel drugs is their biocompatibility with the biological environment. Traditionally, small mammalian models remain the putative method to assess the possible toxicities and biodistribution of nanomaterials in humans. However, zebrafish *Danio rerio* are gaining importance as a biocompatibility model in neurobiology, toxicology, molecular and developmental biology as well as preclinical screening of nanopharmaceuticals.[38] The utility of zebrafish for toxicity screens is largely based upon the close homology with the human genome, as well as physiological and anatomical similarities including the blood brain barrier, endothelial cells, and immunogenic responses.[39] The optical transparency of zebrafish embryos and their fertilization and development outside the mother enable an easy and thorough observation of drug effects on internal organs in vivo as well as body distribution.

Herein, we report the use of capping agents anchored with sterically hindered disulfide bond to control the release rate of a model drug from selected mesoporous material. We show that it is possible to regulate the rate of cargo release by varying the level of hindrance around disulfide bonds connecting MSNs with capping agents. To achieve this goal, MSNs were functionalized with three different linker molecules bearing the disulfide bond with different substituents. The mesopores were loaded with rhodamine B (RB) as a model drug while the pore entrances were closed with β-cyclodextrin (βCD), providing systems with three levels of hindrance around the disulfide bonds. We also show that the system is nonteratogenic with a model vertebrate, zebrafish *Danio rerio*.

EXPERIMENTAL SECTION

Materials and Methods. Chemicals were purchased from the following suppliers: tetraethyl orthosilicate (TEOS), cetyltrimethylammonium bromide (CTAB), dithiothreitol (DTT), 3-mercaptopropionic acid, triethylamine, N-hydroxysuccinimide (NHS), N,N′-dicyclohexylcarbodiimide (DCC), dimethyl sulfoxide-d_6, 4-methylbenzoic acid, dibenzoylperoxide, sodium sulfate, thiourea, anhydrous 1,4-dioxane, anhydrous toluene, ethanol, trichloroethylene, anhydrous N,N-dimethylformamide (DMF), iodine, and ammonium chloride from Sigma-Aldrich; methanol, sodium hydroxide, 2,2′-dipyridyl disulfide (DPDS), acetic acid, dihloromethane, ethyl acetate, 37% hydrochloric acid, imidazole, hexane, 4-toluenesulfonyl chloride, βCD, acetone, RB, and phosphate buffer saline (PBS) tablets from Merck; N-Bromosuccinimide (NBS), triphenylphosphine, and anhydrous acetonitrile from Acros; 4-ethylbenzoic acid from Alfa Aeser and (3-aminopropyl)trimethoxysilane (APTMS) from ABCR.

BET (Brunauer−Emmett−Teller) surface area and BJH (Barrett−Joyner−Halenda) adsorption/desorption curves were acquired via N_2 adsorption/desorption isotherms using Micromeritics ASAP 2020 volumetric adsorption analyzer at 77 K. Scanning electron micrographs were acquired using Zeiss SUPRA 35VP scanning electron microscope (SEM). Low-angle diffractograms were acquired on PANalytical X-Pert PRO high-resolution diffractometer. UV−Vis spectroscopy measurements were performed using a PerkinElmer Lambda 900 instrument and fluorescence spectroscopy measurements using a BioTek Synergy Mx microplate reader. ^{1}H NMR spectra were acquired on a 300 MHz Varian and a 400 MHz Bruker NMR system. Fourier transform infrared spectroscopy (FTIR) spectra were acquired on a Bruker IFS 66/S instrument using KBr pellets. Mass spectroscopy measurements were performed on Waters Q-TOF Premier. Images of zebrafish were acquired using a Leica TCS SP5 inverted laser-scanning microscope on a Leica DMI 6000 CS module (Leica Microsystems) equipped with an objective HCX PL Fluotar L 20×, NA 0.4. RB was excited using a 543-nm laser line of 1.5 mW HeNe laser and emitted light detected between 560 and 630 nm. Transmission electron microscopy (TEM) was performed using Jeol JEM-2100 TEM with a LaB_6 electron source.

Material Synthesis, Functionalization, and Characterization. *MSN Synthesis.* MSNs were synthesized according to Li et al.[40] CTAB (1.0 g) was dissolved in H_2O (480 mL) with stirring. Afterward, a 2 M NaOH solution (3.5 mL) was added and the temperature adjusted to

Scheme 1. Schematics of the Synthetic Procedures Leading to the Six Systems Investigated in This Work[a]

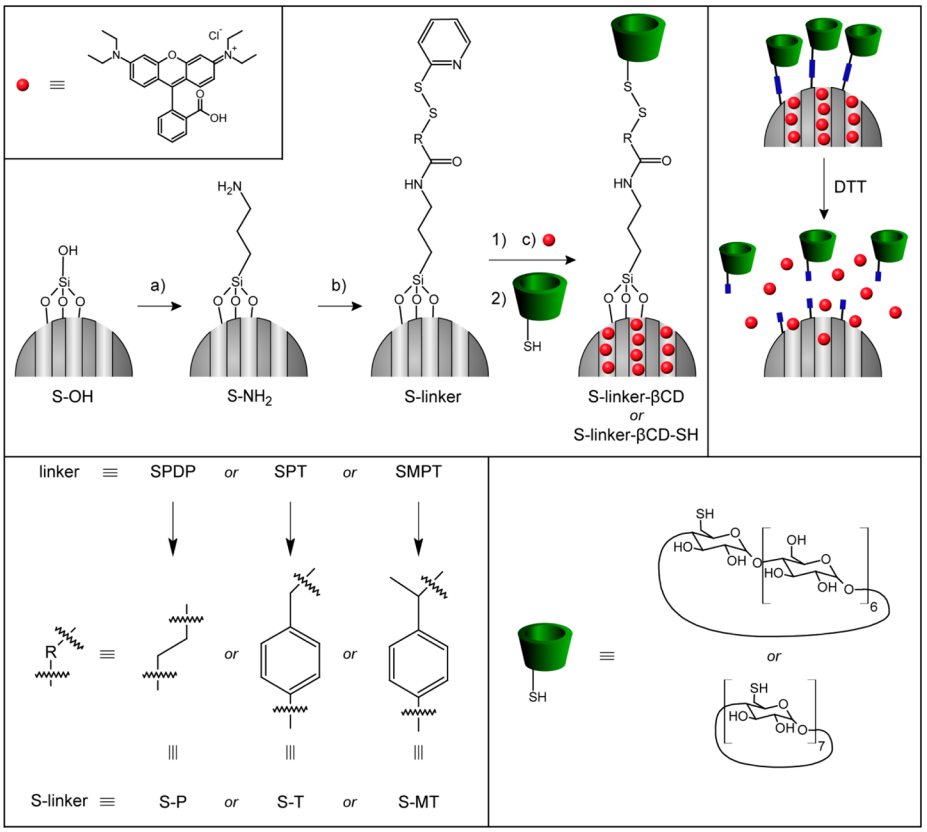

[a]S-linker was combined with either monothio-*β*CD or perthio-*β*CD cap. DTT uncaps the pores and releases the dye. (a) APTMS, (b) linker, (c) dye loading.

80 °C. TEOS (5 mL) was added dropwise over several minutes. After 2 h the suspension was filtered and washed with H_2O and MeOH. As-synthesized MSNs were dried at room temperature. Afterward, CTAB was extracted via solvent extraction. The obtained material was suspended in a mixture of MeOH (160 mL) and hydrochloric acid (9 mL). The suspension was stirred and refluxed overnight under inert atmosphere. After cooling to room temperature, the particles were filtered and washed with MeOH. Solvent-extracted MSNs (S−OH) were dried at 80 °C under high vacuum for 24 h.

MSN Grafting. Solvent-extracted MSNs (1.0 g) were suspended in anhydrous toluene (90 mL) and APTMS in anhydrous toluene (10 mL) was added (see Scheme S3 in the Supporting Information). The suspension was refluxed under inert atmosphere for 16 h. It was then allowed to cool down, filtered, and washed with toluene and MeOH. Product S-NH_2 was dried under a high vacuum.

Functionalization with Linkers. Amino-functionalized MSNs (0.200 g) were suspended in anhydrous MeCN (15 mL). Solution of corresponding linker (N-succinimidyl 3-(2-pyridyldithio)-propionate (SPDP), 4-(succinimidyloxycarbonyl)-*α*-(2-pyridyldithio)toluene (SPT) and 4-(succinimidyloxycarbonyl)-*α*-methyl-*α*-(2-pyridyldithio)-toluene (SMPT)) (0.22 mmol) in anhydrous MeCN (5 mL) was added during stirring at room temperature. After 16 h, the material was filtered and washed with MeCN and MeOH. The products of reactions with SPDP, SPT and SMPT linkers, denoted as S-P, S-T, and S-MT, respectively, were dried under high vacuum.

Determination of Linker Concentration on MSN. Accurately weighed MSNs (~5 mg) were suspended in water and a large excess of DTT was added and stirred for 24 h (see Scheme S4 in the Supporting Information). The solid was separated by centrifugation, the supernatant diluted, and the concentration of 2-thiopyridone determined by UV−vis spectrometry using molar extinction coefficient of ε_{343} = 8.08 × 103 L mol^{-1} cm^{-1} at 343 nm.[41]

Loading of RB. S-P, S-T, and S-MT (0.050 g) were suspended, respectively, in a 2 mM solution of RB in DMF:H_2O (1:1) (9 mL), sonicated and stirred for 24 h. *β*CD-SH (0,072 g) or *β*CD-(SH)7 in the same solvent (1 mL) was added and the stirring continued for 3 days. The resulting red solid was separated with centrifugation and washed with H_2O. Products of the reaction with monothio-*β*CD: S-P-*β*CD, S-T-*β*CD and S-MT-*β*CD; and of the reaction with perthio-*β*CD: S-P-*β*CD-SH, S-T-*β*CD-SH, and S-MT-*β*CD-SH were dried under high vacuum in a desiccator overnight.

Extent of Monothio-βCD Reaction with MSNs. S-P, S-T, and S-MT (0,050 g), respectively, were treated as in the loading process with omission of the dye. After 3 days, the solid was separated with centrifugation and the supernatant diluted with H_2O and analyzed using a UV−vis spectrometer.

RB Content. RB content was determined by dissolving the MSNs (~2 mg) in a 2 M NaOH solution (2 mL), neutralizing it with a 1 M HCl (aq) (4 mL), diluting it with PBS and measuring the concentration of RB.

RB Release. Accurately weighed MSNs with *β*CD (~2 mg) were suspended in a PBS solution (6.0 mL) containing 5 mM DTT or 0 mM DTT (control conditions). The suspension was stirred and the aliquots taken at predetermined times. The procedrure continued by centrifugation and analysis of supernatant on a fluorescence spectrophotometer. The amount of released RB was quantified using a calibration curve obtained with RB solutions of different concentrations. The amount of released RB was then plotted against time with error bars (where present), indicating the standard deviation (n = 3).

Testing of Teratogenic Effects with a Model Vertebrate Zebrafish *Danio rerio*. Experiments with zebrafish were performed as described in Jemec et al.[42] and breeding according to Tišler et al.[43] Briefly, fertilized eggs in the four to eight cell stages were placed in 24-well plates; each well contained 1 mL of test medium. Twenty eggs per

each concentration of nanomaterial's suspension were exposed. Test plates were exposed at 26 °C and under a 12 h light:12 h dark photoperiod. After 24 and 48 h of exposure, lethal malformations (i.e., egg coagulation, missing heartbeat, missing somites, missing tail detachment from the yolk sac), and nonlethal malformations (i.e., no eye and body pigmentation, missing blood flow, spine deformation, yolk sac edema, incomplete eye and ear development) were evaluated. After the embryos have hatched, every day onward up to 4 days post-fertilization, the larvae were observed for the mortality, malformations, and body length using a Nikon DS-Fi1 digital camera and a NIS-Elements Documentation 2.2 imaging software. The body length was measured as a distance from the most anterior part of the head to the tip of the tail, following the path of a developing spinal cord.

Experiments were performed with bare MSNs (0, 2.5, and 25 mg/L dispersed in 0.75 mM NaHCO3) and S-P-βCD-SH (2.5 and 25 mg/L). To avoid excessive animal testing, we evaluated only the system that exhibited the highest amount of RB release (S-P-βCD-SH). For a control, only a 0.75 mM $NaHCO_3$ solution was used. After 4 days of exposure, fluorescence microscopy imaging was conducted to confirm the presence of MSNs inside the zebrafish.

RESULTS AND DISCUSSION

Material Synthesis and Characterization. MCM-41 type MSNs were chosen as a mesoporous support for the envisioned release system. MSNs were synthesized in the basic solution of a templating agent, followed by extraction in acidic MeOH, yielding a mesoporous structure with void pores. MSNs were analyzed with SEM and TEM both of which revealed spherical particles with a diameter of less than 100 nm and a mesoporous structure with parallel pores (see Figures S1 and S2 in the Supporting Information). Low-angle X-ray powder diffraction analysis of solvent-extracted MCM-41 (S−OH) confirmed the hexagonal mesoporous structure with p6mm space group with distinct Bragg peaks that can be indexed as reflections from (100), (110), and (200) planes (see Figure S3 in the Supporting Information). The nitrogen adsorption−desorption isotherm of S−OH showed a typical type IV curve (see Figure S4 in the Supporting Information), characteristic for mesoporous silica.[17] Narrow distribution of pore diameters with a mean value of 3.7 nm was calculated using the BJH model (see Figure S5 in the Supporting Information). The removal of the templating agent was confirmed by elemental analysis.

The pathway of silica modification is outlined in Scheme 1. First, MSNs were grafted with APTMS, introducing amine groups onto silica surface, yielding material denoted S-NH_2. The concentration of amino groups was approximately 0.7 mmol/g as determined from elemental analysis. Next, three different linker molecules, SPDP, SPT and SMPT (see Scheme S5 in the Supporting Information), were attached to S-NH_2, yielding S-P, S-T, and S-MT materials, respectively. All three linkers possess two reactive groups: the succinimidyl group, which was used to form amide bond with amine-functionalized MSNs and the pyridyldithio fragment, which reacts with the thiol group to form the disulfide bond (see Scheme S5 in the Supporting Information). The main difference between linkers is the substituent on the disulfide bond, which introduces a varying degree of hindrance. SPDP possesses the least bulky ethyl substituent; SPT contains a bulkier benzyl substituent while SMPT, in addition to benzyl, also possesses a methyl group on α C atom. Attachment of linkers to MSN surface through the formation of an amide bond was investigated using FTIR (see Figure S6 in the Supporting Information). The peaks at 1564 cm^{-1} (amide II band) and 1422 cm^{-1} (either C−H or C═C aromatic bond) confirm the attachment of linkers. The peak at around 1000 cm^{-1} can be attributed to abundant Si−O bonds in MSNs.

The concentration of grafted linkers on MSNs was determined by cleaving the disulfide bond with DTT and measuring the concentration of released 2-thiopyridone (see Figure 1). Approximately 0.4 mmol/g of linker was graftead onto silica surface. The higher amount of linker in S-P compared to S-T and S-MT can be attributed to the smaller size of SPDP compared to SPT and SMPT, thus enabling a denser packing on the surface.

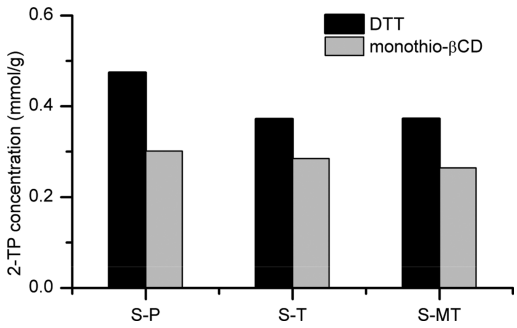

Figure 1. Concentration of released 2-thiopyridone from S-P, S-T, and S-MT by reduction with DTT (black) and by reaction with monothio-βCD (gray).

To determine the extent of reaction with βCD, we reacted monothio-βCD with S-linker MSNs and measured the concentration of released 2-thiopyridone spectrometrically. The analysis showed little difference between the systems, all three exhibiting 0.25−0.30 mmol/g of released 2-thiopyridone. In all cases, the concentrations were lower than with the DTT. Although DTT will form a cyclic compound upon reduction of disulfide bond, monothio-βCD stays attached to the silica, thus imposing a steric hindrance to other monothio-βCD molecules. These results confirm a similar extent of reaction of all S-linker materials with βCD.

To prepare the release systems, we used RB as a model drug. It was loaded into the mesopores by diffusion in a 2 mM solution. Afterward, monothio-βCD and perthio-βCD capping agents were added, respectively, to react with pyridyldithio groups of the S-linker material and form disulfide bond, thus closing the pores and entrapping the dye. The syntheses yielded six systems, as summarized in Table 1.

FTIR analysis of monothio-βCD-functionalized MSNs showed an increase at 2939 cm^{-1} corresponding to the C−H bond (see Figure S7 in the Supporting Information). An absence of the S−H bond peak around 2600 cm^{-1} indicates the attachment of monothio-βCD rather than cleavage of the disulfide without the attachment. Formation of the product between perthio-βCD and S-linker materials revealed a peak at 2570 cm^{-1} assigned to unreacted S−H groups in perthio-βCD and a relative increase of the peak at 2933 cm^{-1} corresponding to C−H bond (see Figure S8 in the Supporting Information). S-P-βCD-SH, as an example of the present functional system, was characterized using TEM. The approximately 1.5 nm thick layer visible on the surface of inorganic silica base is ascribed to the linker and βCD attached to the MSNs surface (see Figure S9 in the Supporting Information). Furthermore, intact pores of S-P-βCD-SH can be seen on the micrograph (see Figure S10 in the Supporting Information). The calculated pore diameter

Table 1. Systems with Encapsulated RB and Capped with Either Monothio-βCD or Perthio-βCD

sample	linker	hindrance level[a]	βCD	RB content (μmol/g)	k_H (μmol/g$\sqrt{\text{min}}$)	R^2
S-P-βCD	SPDP	1	monothio-βCD	9.3	0.21	0.99
S-T-βCD	SPT	2	monothio-βCD	9.2	0.13	0.95
S-MT-βCD	SMPT	3	monothio-βCD	12.8	0.06	0.96
S-P-βCD-SH	SPDP	1	perthio-βCD	11.2	0.31	0.99
S-T-βCD-SH	SPT	2	perthio-βCD	14.4	0.17	0.95
S-MT-βCD-SH	SMPT	3	perthio-βCD	18.6	0.14	0.95

[a]Level 1, ethyl substituent; 2, toluyl substituent; 3, α-methyltoluyl substituent on one side of the disulfide bond.

of 3.4 nm closely matches the diameter of bare MSNs (3.7 nm) as calculated using the BJH model.

Release Testing. RB release testing was performed in a PBS buffer in the presence of 5 mM DTT and in its absence (control conditions). The suspension of nanoparticles was stirred and the aliquots withdrawn at specific times. After centrifugation the concentration of RB in supernatants was determined with fluorescence spectroscopy. All systems exhibited a small burst-release of RB at the beginning of the experiment, which can be attributed to a fast release of RB adsorbed onto MSNs' outer surface after the interaction of dried material with the buffer medium (Figures 2a and 3a).

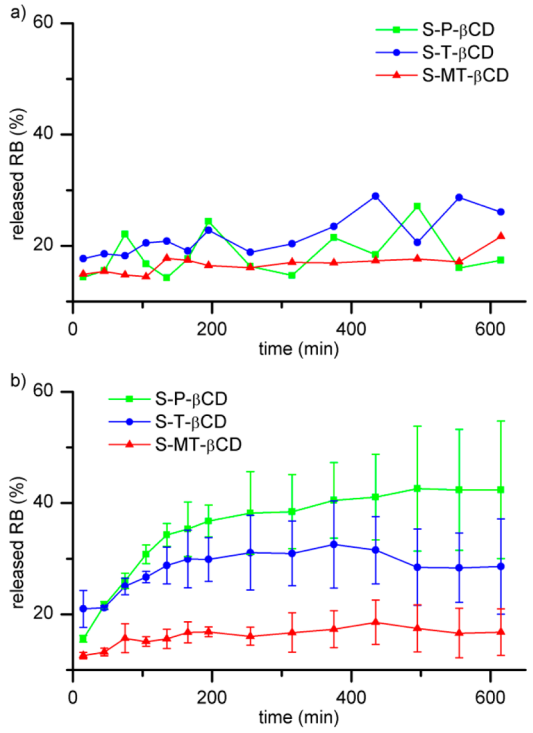

Figure 2. Release of RB from S-P-βCD, S-T-βCD, and S-MT-βCD (a) in the absence of DTT and (b) in the presence of 5 mM DTT.

Nevertheless, the amount of RB release in control conditions was almost constant over a period of 10 h, indicating a good capping of mesopores by βCD. In the presence of DTT the release curves of S-linker-βCD systems exhibited characteristics typical for mesoporous materials, with a distinct difference between the three systems with different linkers (Figure 2b).[16,44] Different amounts of RB are released as a consequence of linkers having different half-life in the same environment. At about t = 300 min, the start of plateau region can be observed.

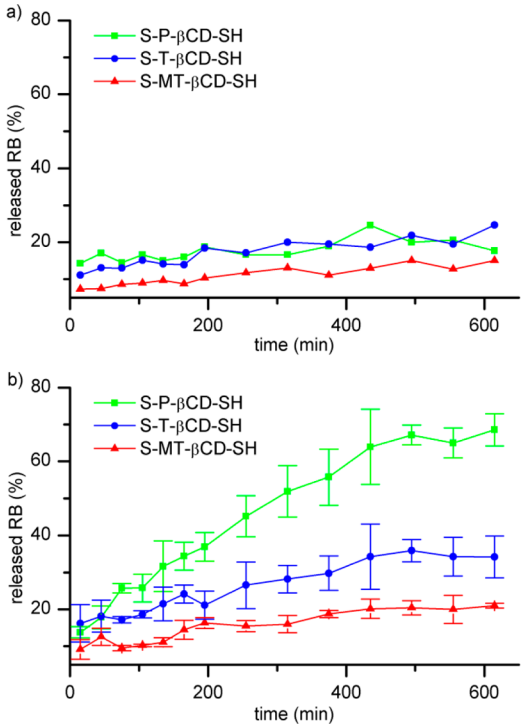

Figure 3. Release of RB from S-P-βCD-SH, S-T-βCD-SH, and S-MT-βCD-SH (a) in the absence of DTT and (b) in the presence of 5 mM DTT.

The systems bearing perthio-βCD (Figure 3b) show a higher RB release compared to the S-linker-βCD systems. The systems exhibit different release profiles associated with level of hindrance of the disulfide bond. Likewise, the increasing total amount of released RB can be associated with the decreasing level of hindrance of the linker used in the synthesis. S−P loaded with RB but without the attachment of βCD exhibited a poorer DTT-responsive release as notable leakage was observed in absence of DTT (see Figure S11 in the Supporting Information). The difference between the control and the DTT-treated sample can be attributed to a $\pi-\pi$ stacking of the pyridyl moiety of the linker and RB.

Release rates from MSNs in the presence of DTT can be analyzed using the Higuchi model,[45] which has already been successfully applied to model the release rate of cargo from mesoporous silica.[23] In this model, the amount of released cargo per mass of sample Q_t is proportional to the square root of time t

$$Q_t = k_H\sqrt{t} \quad (1)$$

where k_H is a constant. In our particular case, there was an initial small burst-release, so eq 1 was modified accordingly

$$Q_t = k_H\sqrt{t} + c_0 \quad (2)$$

where c_0 is the amount of RB released at t = 0 min. Fits to the measured curves using eq 2 are displayed in Figure 4. Analysis

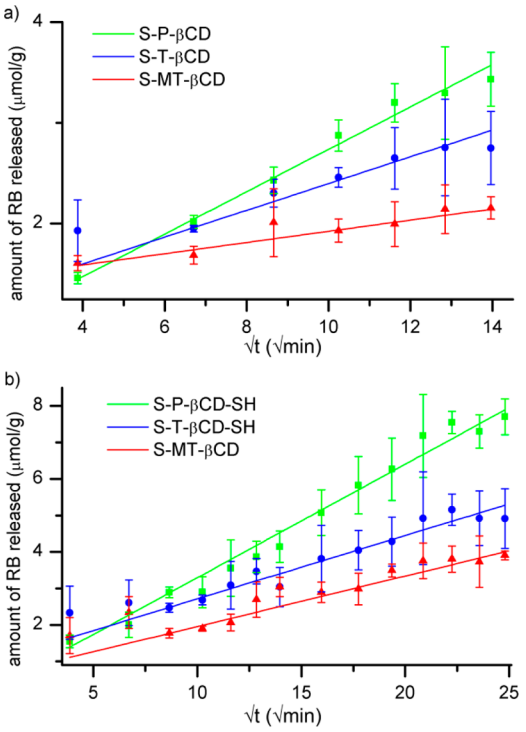

Figure 4. Linear fit of RB release in 5 mM DTT to Higuchi model: (a) S-linker-βCD and (b) S-linker-βCD-SH.

of fitted values reveals an inverse dependence of k_H on the level of hindrance of the disulfide bond (Table 1). Coefficient of determination (R^2) is equal to or higher than 0.95, indicating a good fit of data to the model.

It can be seen that k_H decreases by a factor 1.6 and 2.2 when going from S-P-βCD to S-T-βCD and from S-T-βCD to S-MT-βCD, respectively. In S-linker-βCD-SH systems, a decrease by factor 1.8 and 1.2 from S-P-βCD-SH to S-T-βCD-SH and from S-T-βCD-SH to S-MT-βCD-SH, respectively, was calculated. This decrease in k_H indicates that the slower release rate is consistent with the increased hindrance of the disulfide bond in the systems. The release rate of cargo from capped mesoporous systems are controlled not only by the rate of removal of capping agent but also by the pore wall−cargo interaction,[17] which explains the smaller difference between linkers than would be expected on the basis of the half-lives of hindered disulfide bonds alone.

Zebrafish experiments. To evaluate teratogenicity of the synthesized materials, we performed in vivo testing on zebrafish (*Danio rerio*). To avoid excessive animal testing, we evaluated only the system that exhibited the highest amount of RB release (S-P-βCD-SH). Testing was performed using two concentrations of MSNs in medium, namely 2.5 and 25 mg/L. Bare MSNs and the medium without MSNs were used as a control. Zebrafish embryos and later hatched zebrafish were monitored and checked for sublethal and lethal effects on development during 4 days (see Table S1 in the Supporting Information). Effects higher than 10% are considered consequences of toxic effects of material.[46] None of the materials reached this threshold, indicating nonteratogenic nature of bare MSNs and, more importantly, confirming that functionalization of MSNs with βCD did not negatively influence these properties.

None of the tested samples affected hatching of larvae as 100% of hatching success was observed at 4 days post fertilization in all samples. Likewise, no effects on the fish length were observed at 4 days post fertilization. The average fish body length of control animals was 3.35 + 0.14 mm and the averages of body length of fish exposed to tested samples were not significantly different from the control ($p > 0.05$). Our results are in accordance with the findings published by Sharif et al.,[3] who showed that the injection of 35−40 nL (10 mg/mL) of custom-synthesized, fluorescently tagged 200 nm

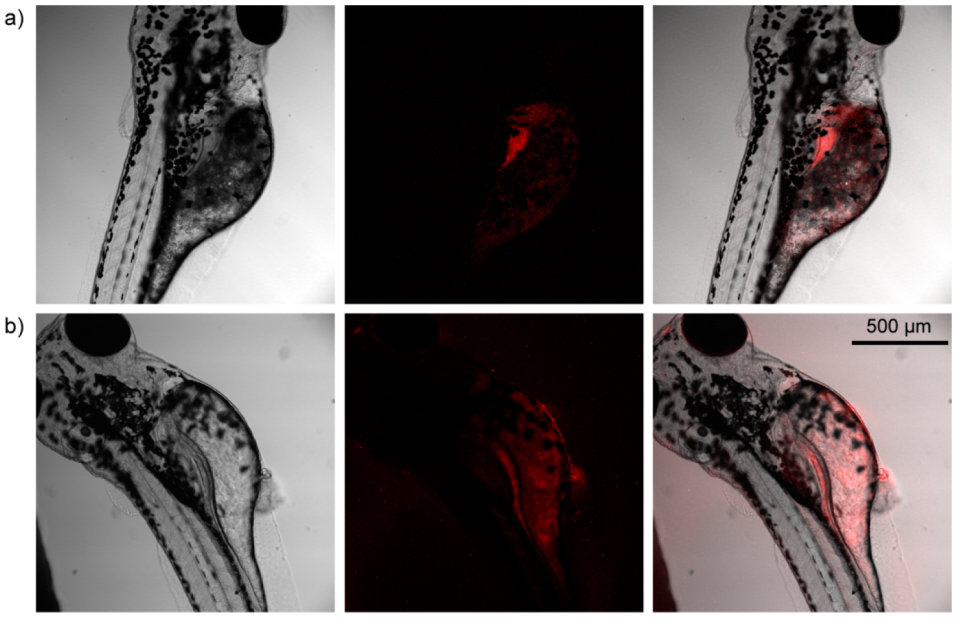

Figure 5. Confocal microscope images of zebrafish after exposure to (a) 2.5 mg/L and (b) 25 mg/L S-P-βCD-SH for 4 days. Left: visible light image, center: fluorescence from RB, right: overlaid images. Scale bar is valid for all images.

MSNPs into the left flank, behind the yolk sac extension, of 2-day-old zebrafish embryos did not significantly affect embryo development and survival. They also showed no significant cell death. 96 h post-fertilization hatched zebrafish were visualized under confocal microscope to confirm the presence of MSNs in zebrafish. RB loaded MSNs were located inside the zebrafish yolk sac, while a minimal amount of MSNs was detected elsewhere (Figure 5).

CONCLUSIONS

We have synthesized six model stimulus-responsive drug delivery systems based on mesoporous silica containing three cleavable linkers with varying level of hindrance around the disulfide bonds. Pore voids were loaded with a model drug (RB) and two βCD derivatives, monothio-βCD and perthio-βCD, were attached to prevent diffusion of the dye. The release of the dye in presence of DTT was dependent on the level of hindrance around the disulfide bond. The systems with greater level of hindrance exhibited a slower release with a smaller amount of cargo released after 10 h in the same environment. The release curves were successfully fitted to the Higuchi model. Moreover, the calculated Higuchi constants revealed an approximately 2-fold decrease of the constant for each increased level of hindrance, resulting in an altered and controllable release of the model drug. By varying the level of hindrance around the disulfide bonds we have demonstrated the possibility of achieving different release rates and amounts released in the same environment by only minor structural differences between the systems. At the same time, all of these systems exhibited a stimulus-responsive behavior.

To maximize the therapy efficiency, drugs need to be administered in different regimes exhibiting different release profiles and in different amounts. Altering the environment in the course of drug administration is usually not desired or possible at all. Therefore, drug delivery systems with intrinsic control over the release rate are favored. Further testing of MSNs on zebrafish embryos confirmed uptake of nanoparticles into gastro-intestinal track. No sublethal and lethal effects of the material on the zebrafish during 96 h of exposure were detected, confirming nonteratogenicity of bare MSNs as well as RB-loaded MSNs. The synthesized model systems present a promising way to achieve a stimulus-responsive release of the cargo with different release profiles in the same environment. Because the drug's effects and physiological responses are closely related to the release rate and amount of the drug in the body, the present study creates another stepping stone in the road toward optimizing the effectiveness of the administered drugs.

ASSOCIATED CONTENT

Supporting Information

Linker syntheses, βCD derivatives syntheses, and additional results. This material is available free of charge via the Internet at http://pubs.acs.org.

AUTHOR INFORMATION

Corresponding Author

*Tel: +386 1 4760 320. Fax: +386 1 4760 300. E-mail: miran.gaberscek@ki.si.

Present Addresses

[§]Uroš Maver is currently at Faculty of Medicine, University of Maribor, Slomškov trg 15, 2000 Maribor, Slovenia

[#]Anita Jemec is currently at Biotechnical faculty, University of Ljubljana, Jamnikarjeva 101, 1000 Ljubljana, Slovenia

Notes

The authors declare no competing financial interest.

ACKNOWLEDGMENTS

Financial support from the Slovenian Research Agency is acknowledged. The authors thank Dr. Boštjan Genorio for help with β-cyclodextrin derivatization, Edi Kranjc for XRD measurement, Dr. Iva Hafner Bratkovič for help with spectroscopy measurements, and Aleksandar Gaćeša for ^{13}C NMR measurement.

ABBREVIATIONS

MSN, mesoporous silica nanoparticle
GSH, glutathione
RB, rhodamine B
βCD, β-cyclodextrin
TEOS, tetraethyl orthosilicate
CTAB, cetyltrimethylamonium bromide
DTT, dithiothreitol
NHS, N-hydroxysuccinimide
DCC, N,N′-dicyclohexylcarbodiimide
DMF, N,N-dimethylformamide
DPDS, 2,2′-dipyridyl disulfide
PBS, phosphate buffer saline
NBS, N-bromosuccinimide
APTMS, (3-aminopropyl)trimethoxysilane
FTIR, Fourier transform infrared spectroscopy
SPDP, N-succinimidyl 3-(2-pyridyldithio)-propionate
SPT, 4-(succinimidyloxycarbonyl)-α-(2-pyridyldithio)-toluene
SMPT, 4-(succinimidyloxycarbonyl)-α-methyl-α-(2-pyridyldithio)toluene
SEM, scanning electron microscope
TEM, transmission electron microscopy
BET, Brunauer–Emmett–Teller
BJH, Barrett–Joyner–Halenda

REFERENCES

(1) Mal, N. K.; Fujiwara, M.; Tanaka, Y. *Nature* **2003**, *421*, 350–353.
(2) Lai, C.-Y.; Trewyn, B. G.; Jeftinija, D. M.; Jeftinija, K.; Xu, S.; Jeftinija, S.; Lin, V. S.-Y. *J. Am. Chem. Soc.* **2003**, *125*, 4451–4459.
(3) Sharif, F.; Porta, F.; Meijer, A. H.; Kros, A.; Richardson, M. K. *Int. J. Nanomed.* **2012**, *7*, 1875–1890.
(4) Yang, P.; Gai, S.; Lin. *J. Chem. Soc. Rev.* **2012**, *41*, 3679–3698.
(5) Bruhwiler, D. *Nanoscale* **2010**, *2*, 887–892.
(6) Yang, Y.-W. *Med. Chem. Commun.* **2011**, *2*, 1033–1049.
(7) Li, Z.; Barnes, J. C.; Bosoy, A.; Stoddart, J. F.; Zink, J. I. *Chem. Soc. Rev.* **2012**, *41*, 2590–2605.
(8) Yuan, Q.; Zhang, Y.; Chen, T.; Lu, D.; Zhao, Z.; Zhang, X.; Li, Z.; Yan, C.-H.; Tan, W. *ACS Nano* **2012**, *6*, 6337–6344.
(9) Silveira, G. Q.; Vargas, M. D.; Ronconi, C. M. *J. Mater. Chem.* **2011**, *21*, 6034–6039.
(10) Guo, W.; Wang, J.; Lee, S.-J.; Dong, F.; Park, S.; Ha, C.-S. *Chem.—Eur. J.* **2010**, *16*, 8641–8646.
(11) Porta, F.; Lamers, G. E. M.; Zink, J. I.; Kros, A. *Phys. Chem. Chem. Phys.* **2011**, *13*, 9982–9985.
(12) Guo, R.; Li, L.-L.; Zhao, W.-H.; Chen, Y.-X.; Wang, X.-Z.; Fang, C.-J.; Feng, W.; Zhang, T.-L.; Ma, X.; Lu, M.; Peng, S.-Q.; Yan, C.-H. *Nanoscale* **2012**, *4*, 3577–3583.
(13) Zhu, Y.; Fujiwara, M. *Angew. Chem., Int. Ed.* **2007**, *46*, 2241–2244.

(14) Agostini, A.; Sancenón, F.; Martínez-Máñez, R.; Marcos, M. D.; Soto, J.; Amorós, P. *Chem.—Eur. J.* **2012**, *18*, 12218−12221.
(15) Aznar, E.; Mondragón, L.; Ros-Lis, J. V.; Sancenón, F.; Marcos, M. D.; Martínez-Máñez, R.; Soto, J.; Pérez-Payá, E.; Amorós, P. *Angew. Chem., Int. Ed.* **2011**, *50*, 11172−11175.
(16) Patel, K.; Angelos, S.; Dichtel, W. R.; Coskun, A.; Yang, Y.-W.; Zink, J. I.; Stoddart, J. F. *J. Am. Chem. Soc.* **2008**, *130*, 2382−2383.
(17) Ukmar, T.; Maver, U.; Planinšek, O.; Kaučič, V.; Gaberšček, M.; Godec, A. *J. Controlled Release* **2011**, *155*, 409−417.
(18) Horcajada, P.; Rámila, A.; Pérez-Pariente, J.; Vallet-Regí, M. *Microporous Mesoporous Mater.* **2004**, *68*, 105−109.
(19) Andersson, J.; Rosenholm, J.; Areva, S.; Lindén, M. *Chem. Mater.* **2004**, *16*, 4160−4167.
(20) Qu, F.; Zhu, G.; Huang, S.; Li, S.; Sun, J.; Zhang, D.; Qiu, S. *Microporous Mesoporous Mater.* **2006**, *92*, 1−9.
(21) Muñoz, B.; Rámila, A.; Pérez-Pariente, J.; Díaz, I.; Vallet-Regí, M. *Chem. Mater.* **2003**, *15*, 500−503.
(22) Doadrio, J. C.; Sousa, E. M. B.; Izquierdo-Barba, I.; Doadrio, A. L.; Perez-Pariente, J.; Vallet-Regi, M. *J. Mater. Chem.* **2006**, *16*, 462−466.
(23) Aznar, E.; Sancenón, F.; Marcos, M. D.; Martínez-Máñez, R.; Stroeve, P.; Cano, J.; Amorós, P. *Langmuir* **2012**, *28*, 2986−2996.
(24) Zhang, Q.; Liu, F.; Nguyen, K. T.; Ma, X.; Wang, X.; Xing, B.; Zhao, Y. *Adv. Funct. Mater.* **2012**, *22*, 5144−5156.
(25) Cui, Y.; Dong, H.; Cai, X.; Wang, D.; Li, Y. *ACS Appl. Mater. Interfaces* **2012**, *4*, 3177−3183.
(26) Bernardos, A.; Aznar, E.; Coll, C.; Martínez-Mañez, R.; Barat, J. M.; Marcos, M. D.; Sancenón, F.; Benito, A.; Soto, J. *J. Controlled Release* **2008**, *131*, 181−189.
(27) Zhao, Y.; Trewyn, B. G.; Slowing, I. I.; Lin, V. S.-Y. *J. Am. Chem. Soc.* **2009**, *131*, 8398−8400.
(28) Chen, L.; Wen, Y.; Su, B.; Di, J.; Song, Y.; Jiang, L. *J. Mater. Chem.* **2011**, *21*, 13811−13816.
(29) Park, C.; Kim, H.; Kim, S.; Kim, C. *J. Am. Chem. Soc.* **2009**, *131*, 16614−16615.
(30) Bernardos, A.; Mondragón, L.; Aznar, E.; Marcos, M. D.; Martínez-Máñe, R.; Sancenón, F.; Soto, J.; Barat, J. M.; Pérez-Payá, E.; Guillem, C.; Amorós, P. *ACS Nano* **2010**, *4*, 6353−6368.
(31) Gruenhagen, J. A.; Lai, C.-Y.; Radu, D. R.; Lin, V. S.-Y.; Yeung, E. S. *Appl. Spectrosc.* **2005**, *59*, 424−431.
(32) Xing, R.; Lin, H.; Jiang, P.; Qu, F. *Colloids Surf., A* **2012**, *403*, 7−14.
(33) Saito, G.; Swanson, J. A.; Lee, K.-D. *Adv. Drug Delivery Rev.* **2003**, *55*, 199−215.
(34) Navath, R. S.; Kurtoglu, Y. E.; Wang, B.; Kannan, S.; Romero, R.; Kannan, R. M. *Bioconjugate Chem.* **2008**, *19*, 2446−2455.
(35) Thorpe, P. E.; Wallace, P. M.; Knowles, P. P.; Relf, M. G.; Brown, A. N. F.; Watson, G. J.; Knyba, R. E.; Wawrzynczak, E. J.; Blakey, D. C. *Cancer Res.* **1987**, *47*, 5924−5931.
(36) Thorpe, P. E.; Wallace, P. M.; Knowles, P. P.; Relf, M. G.; Brown, A. N. F.; Watson, G. J.; Blakey, D. C.; Newell, D. R. *Cancer Res.* **1988**, *48*, 6396−6403.
(37) Kellogg, B. A.; Garrett, L.; Kovtun, Y.; Lai, K. C.; Leece, B.; Miller, M.; Payne, G.; Steeves, R.; Whiteman, K. R.; Widdison, W.; Xie, H.; Singh, R.; Chari, R. V. J.; Lambert, J. M.; Lutz, R. J. *Bioconjugate Chem.* **2011**, *22*, 717−727.
(38) Fako, V. E.; Furgeson, D. Y. *Adv. Drug Delivery Rev.* **2009**, *61*, 478−486.
(39) Pyati, U. J.; Look, A. T.; Hammerschmidt, M. *Semin. Cancer Biol.* **2007**, *17*, 154−165.
(40) Li, Z.; Nyalosaso, J. L.; Hwang, A. A.; Ferris, D. P.; Yang, S.; Derrien, G.; Charnay, C.; Durand, J.-O.; Zink, J. I. *J. Phys. Chem. C* **2011**, *115*, 19496−19506.
(41) Na, D. H.; Woo, B. H.; Lee, K. C. *Bioconjugate Chem.* **1999**, *10*, 306−310.
(42) Jemec, A.; Djinović, P.; Tišler, T.; Pintar, A. *J. Hazard. Mater.* **2012**, *219−220*, 213−220.
(43) Tišler, T.; Jemec, A.; Mozetič, B.; Trebše, P. *Chemosphere* **2009**, *76*, 907−914.
(44) He, D.; He, X.; Wang, K.; Chen, M.; Cao, J.; Zhao, Y. *J. Mater. Chem.* **2012**, *22*, 14715−14721.
(45) Higuchi, T. *J. Pharm. Sci.* **1963**, *52*, 1145−1149.
(46) . *ISO 15088:2007, Water Quality—Determination of the Acute Toxicity of Waste Water to Zebrafish Eggs (Danio rerio)*; International Organization for Standardization: Geneva, Switzerland, 2007.